TERMIS — termis.

Tissue Engineering
& Regenerative Medicine
International Society

ORIGINAL ARTICLE

Hydroxyapatite/Collagen Three-Dimensional Printed Scaffolds and Their Osteogenic Effects on Human Bone Marrow-Derived Mesenchymal Stem Cells

Qing Li, DDS, PhD,[1,2] Xiongxin Lei, MD,[3,4] Xiaofei Wang, DDS, PhD,[1,2] Zhigang Cai, DDS, PhD,[2,5] Peijun Lyu, DDS, PhD,[1,2] and Guifeng Zhang, PhD,[3]

Three-dimensional (3D) printing provides a novel approach to repair bone defects using customized biomimetic tissue scaffolds. To make a bone substitute closest to natural bone structure and composition, two different types of hydroxyapatite, Nano hydroxyapatite (nHA) and deproteinized bovine bone (DBB), were dispersed into collagen (CoL) to prepare the bioink for 3D printing. In doing so, a porous architecture was manufactured with 3D printing technology. The physical and chemical properties of the materials were evaluated, including biocompatibility and effect on the osteogenic differentiation of the human bone marrow-derived mesenchymal stem cells (hBMSCs). The XPS, XRD, FTIR, and the mechanical analysis of the material indicated that the two HA were consistent in their elements, but different in their chemical bonds and crystal phases. The SEM results showed the different surface morphologies of the HA crystals as well as the scaffolds, which would be the main factors affecting the internal porous structure of the scaffold. There were no differences between the two composite scaffolds in cell proliferations. FITC-phalloidin/vinculin/DAPI staining indicated that hBMSCs can adhere well to the 3D-printed surfaces. Alkaline phosphatase (ALP) staining reflected ALP expressed on both of the osteogenic-induction medium (OM) group, but not on proliferation medium (PM) group. The real-time polymerase chain reaction results showed the expression levels of osteogenesis-related genes *RUNX2, SOX9, OCN,* and *COL1A1* in OM group were significantly increased after 7 days compared with the PM group ($p < 0.01$). The expression of *SOX9, OCN,* and *COL1A1* in nHA/CoL scaffolds was higher than that in CoL scaffolds ($p < 0.05$). The expression of *OCN* and *COLIA1* in DBB/CoL scaffolds was higher than that in CoL scaffolds ($p < 0.05$). In conclusion, the physicochemical and biological properties of 3D bioprinted scaffolds consisting of nHA/CoL or DBB/CoL would be well suited for the scaffolds to being a porous customized bone substitute, 3D printing scaffolds would be a prospective candidate for clinical application in future.

Keywords: collagen, nano-hydroxyapatite, deproteinized bovine bone, 3D printing, scaffold, osteogenesis differentiation

Impact Statement

Bone loss due to trauma, inflammation, and surgical processes has posed great difficulty in the aesthetic reconstruction of a functional alveolar bone. Tissue engineering and biomaterials, which can promote alveolar bone regeneration, have become a popular focus of current studies. Three-dimensional (3D) printing provides a novel approach to repair bone defects using customized biomimetic tissue scaffolds. Nano hydroxyapatite (nHA) and deproteinized bovine bone (DBB) are two materials mainly used in clinical practice, particularly DBB are widely used in dentistry and craniomaxillofacial orthosis because of the porosity characteristic. To make a bone substitute closest to natural bone structure and composition, nHA and DBB were dispersed into collagen (CoL) to prepare the bioink for 3D printing. The physicochemical and biological properties between the two 3D printing scaffolds were compared. Both nHA/CoL and DBB/CoL 3D printing scaffold would be promising candidate for the clinical applications in the future.

[1]Center of Digital Dentistry, Peking University School and Hospital of Stomatology, Beijing, China.
[2]National Engineering Laboratory for Digital and Material Technology of Stomatology, Beijing, China.
[3]State Key Laboratories of Biochemical Engineering, Institute of Process Engineering, Beijing, China.
[4]College of Chinese Medicine, Beijing University of Chinese Medicine, Beijing, China.
[5]Department of Oral and Maxillofacial Surgery, Peking University School and Hospital of Stomatology, Beijing, China.

Introduction

Iɴ ᴛʜᴇ ᴘᴀsᴛ ᴅᴇᴄᴀᴅᴇ, significant advances have been made in three-dimensional (3D) printing technology, and the customized repair of bone defects has been applied successfully in clinics with metal laser printers.[1] The merits of 3D printing scaffolds include low complication risk, short operational time, and good molding effect during surgery.[2–4] Compared with conventional metal printing or rapid prototyping, 3D bioprinting has been used to fabricate hydroxyapatite bound by different kinds of adhesive polymer scaffolds (CPS). The biodegradable of these polymer materials are able to guide the bone regeneration *in situ*.[5,6] Among these, low temperature 3D bioprinting (LT-3DP) has been considered to be the most suitable method for bone defects repairs in the future, because it was used to generate a 3D blueprint of the patient's specific defects with high biocompatibility materials that are similar with the natural bone component and construction.[7]

As a bone tissue engineering technology, the primary advantage of LT-3DP CPS is the potential to create polymer-mineral composites with enhanced material properties.[8] Also, the LT-3DP has great potential to fabricate tissues with multiple biocomposite materials and cell types, all of which are extremely important for the advancement of bone tissue engineering. Moreover, 3D porous scaffold designs are conducive to cell–matrix interactions and more efficient blood vessels in growth.[9,10]

To mimic the architecture of bone trabecular in LT-3DP, nano hydroxyapatite (nHA) is a good candidate for an appetite substitute of natural bone because of its high osteoconductive activity. Another alternative is a xenogenous bone, such as the deproteinized bovine bone (DBB), which is morphologically and structurally similar to human cancellous bone. Heat treatment has been suggested as an option to obtain protein-free bovine bone.[11] The crystalline phase composition of sintered bovine bone is similar to natural bone mineral that is composed of hydroxyapatite at about 93wt% and about 7wt% β-tricalcium phosphate $(Ca_3(PO_4)_2, β\text{-}TCP)$.[11] The heat-treated bovine bone has an interconnective porous structure (up to about 70vol% porosity) similar to the natural bone, hence allows faster bone in-growth.[12] Moreover, the hydroxylapatite obtained from bone and derived from powder processing has great potential as a bone substitute owing to its excellent biocompatible and osteoconductive properties.[13,14]

Usually, LT-3DP provides the potential to create composites with synthetic or biological polymers, such as collagen.[15] Type I collagen (CoL-I) is the most abundant structural protein in the human body, and an important component of bone tissue. Collagen is also a critical component of bone extracellular matrix, where it plays important roles in the mineralized tissue's strength and toughness. It has been shown that incorporating collagen into mineralized bone cements could enhance their biomechanical properties. Collagen can induce the mineral deposition, and its surface contains sites that promote osteoblast adsorption and mineral deposition. Moreover, it can effectively enhance the mineralization process and develop new bone in the implanted artificial bone scaffold.[16] This kind of polymer can retain but does not occlude the osteoinductive calcium phosphate component and has osteoconductive and osteoinductive characteristics.[17] For example, collagen incorporation into hand-mixed hydroxyapatite has been shown to improve cellular attachment, viability, proliferation, and activity as well as mechanical properties.[17,18]

In this study, nHA and DBB were mixed with CoL-I into biocomposite hydrogel, respectively, to create two types of bioinks. To build up a porous bone scaffold within the biomimetic component, as well as the trabecula construction, the two bioinks were printed with the LT-3DP technology. BMSCs were used to observe the topographies and morphologies of cells adherence on the two 3DP scaffolds. The cellular biocompatibility, including the proliferation and osteogenic differentiation, were compared and evaluated. The application of two hydrogels used as ''bioinks'' in LT-3DP and these biological properties were compared and evaluated.

Materials and Methods

Preparation of DBB

DBB was prepared by calcining bovine cancellous bone following the method of Wang.[19] In brief, the bovine bone was cut into small cubes, and successively being incubated in H_2O_2 solution and stewed in a NaOH solution to remove collagen and proteins. The bone cubes were then washed with water, immersed in H_3PO_4 solution, and heated, respectively. This was followed by washing with absolute ethyl alcohol to remove moisture. After that, the bone cubes were air-dried and heated up to 1000°C. Finally the bone cubes were ground and filtered through a 120-screen cloth to obtain DBB particles with a diameter of 105–125 μm.[19]

Properties of hydroxyapatite

The nHA (Aladdin) (≥Alad <100 nm particle size) and DBB samples were mounted on conductive adhesive tape and sputter coated with Au, and then observed using a scanning electron microscopy (SEM) (JSM 6700F, Japan) at a magnification between 1000× and 10,000×. The composition of the nHA and DBB were investigated by X-ray photoelectron spectroscopy (XPS) (ESCALAB 250Xi USA) using a monochromatic Al Kα source (10 mA, 15 kV).

Preparation of the bioink

The bioinks were divided into three groups, which were, respectively, CoL, nHA/CoL, and DBB/CoL groups. Type I bovine tendon collagen sponge (Collagen Biotechnology Co. Ltd., China) was dispersed in acetic acid of 0.05 mol/mL at a concentration of 3 g/100 mL, then collagen gel was gotten to be the CoL group. nHA and DBB were, respectively, added into the collagen gel with constant stirring at 45 rpm for 12 h at 4°C temperature, the nHA/CoL and DBB/CoL bioink were obtained.[20] The concentration of the HA in biocomposite ink was 0.75 g/100 mL.

Three-dimensional bioprinting

The 3D Bioplotter (Envision Tec, Germany) was used to produce the 3D bioprinting scaffolds. For building 3D construction, the cuboid model was designed by Image ware 13.1. The distance between each printed line was 1.5 mm. The hydrogel scaffolds were fabricated by layer-by-layer

deposition, and a $15 \times 15 \times 5 \, mm^3$ architecture was gotten (Fig. 1A, B). The parameters of the 3D Bioplotter were determined after repeated printing experimentations to ensure the consistency and repeatability of the 3D bioprinted constructions. Related parameters are presented in Table 1. When each printed scaffold was completed, freeze-drying was conducted to obtain the freeze-dried scaffolds. After that, the scaffolds were crosslinked with 0.2% glutaraldehyde solution (80% ethanol aqueous solution) for 2 h at room temperature, then rinsed in deionized water several times to remove residual glutaraldehyde. The crosslinked scaffolds were put into freeze-dryer again to get the final specimen. The sterile operations were carried out during the processes.

SEM of the 3D bioprinting scaffold

The freeze-dried scaffolds were coated with Au and investigated with SEM at a magnification between $100 \times$ and $2000 \times$ as the method of ''Properties of hydroxyapatite'' above.

Fourier transform infrared spectroscopy analysis

The chemical composition of the scaffolds was investigated by Fourier transform infrared spectroscopy (FTIR; Spectrum GX). Each of samples was ground together with KBr at a rate about 1:20 in an agate mortar and compressed to tablets. The spectra ranges were set as 4000 to $400 \, cm^{-1}$ with a resolution of $4 \, cm^{-1}$, and the scan time was about 100 s. Pure collagen sponge served as a reference.

X-ray diffraction analysis

The scaffolds lyophilized were cut into small cubes at $20 \times 20 \times 2 \, mm$, and gently flattened before analysis. The crystal phase compositions of each scaffold were investigated by X-ray diffraction (XRD, SmartLab X, Japan). The materials XRD spectra were taken using nickel-filtered Cu $K\alpha$ radiation at 40 kV and 200 mA. Spectra were recorded from $2\theta = 5°$ to $90°$ at a scanning speed of $15°/min$ and a step size of $0.02°$. nHA and DBB powder served as a reference and was heated to $100°C$ for 12 h before use.

Mechanical properties of scaffolds

The Young's modulus of the three groups of scaffold were determined using a Universal Testing Machine (Instron 300DX, US). The dimensions of each specimen were measured using a vernier caliper before detection. Then, the scaffolds were placed on the detecting platform and loaded at the rate of 1 mm/min until the scaffolds crushed. The force and displacement data were recorded to generate the stress–strain curves. By measuring the slope of the stress–strain curve in the elastic region, Young's modulus could be calculated. Each group was detected five times, and the results are displayed in the form of mean ± standard deviation.

Evaluation of the biological characteristics of the bioprinting materials

Cell culture. Human bone marrow-derived mesenchymal stem cells (hBMSCs) were purchased from ScienCell (ScienCell) and cultured in 10 cm dishes with Dulbecco's modified Eagle's medium (DMEM) supplemented with 10%

(v/v) fetal bovine serum (FBS) in incubator ($37°C$, 5% CO_2 and 100% relative humidity). The medium was changed three times a week until passage 3 (P3). After being digested and counted, the cell suspension was concentrated and suspended in DMEM (10% FBS) to adjust the cell number to $6 \times 10^7/mL$. After placing the sterile 3D printing scaffolds in a 24-well culture plate and wetting the materials with proliferation medium (PM) beforehand, each scaffold sample was seeded with $100 \, \mu L$ of cell suspension. After 4 h of cell adhesion to the scaffold in incubator, $900 \, \mu L$ of DMEM (10% FBS) was added to each well. The medium was replaced every other day.

Immunofluorescence staining. The immunofluorescence staining of hBMSCs cytoskeleton was conducted. After 24 h of incubation on each scaffold, the cells were fixed in 4% paraformaldehyde for 10 min at room temperature, permeabilized with 0.1% TritonTMX-100 PBS solution for 5 min, and blocked using 1% bovine serum albumin (BSA) for 30 min at room temperature. Then, the cells were incubated with FITC-phalloidin (Sigma-Aldrich) at a concentration of $5 \, \mu g/mL$ with each well 0.5 mL for 30 min, followed by incubation in DAPI ($5 \, \mu g/mL$) for 5 min in the dark at room temperature. Each incubation was followed by three times of PBS washing. Confocal Laser Scanning Microscope (CLSM, Olympus IX71, Fluoview, Japan) was used to observe the images.[21]

Vinculin staining. The vinculin staining of the hBMSCs was conducted to observe the cell adhesion on scaffold. After fixed and permeabilized, 3% hydrogen peroxide was added for 10 min and then 3% goat serum was added for 1 h at $4°C$. First antibody of vinculin was added at a scale of 1:200 dilute solutions for the night. Second antibody was added at a scale of 1:500 dilution solutions for 1 h in the dark. With PBS washes after incubation, the cells were counterstained with DAPI for nuclear staining and visualized using a CLSM.

Cell proliferating assay

P3 hBMSCs were counted after digested, centrifuged, and resuspended. The cell suspension was added into each scaffolds, with 1, 5000 cells each well ($n = 5$). After culturing for 1, 3, 5, and 7 days, cell proliferation was determined using the CCK-8 method. The Optical Density (OD) was measured at 450 nm using a microplate reader (Bio-Kinetics Reader, Bio-Tek Instruments). Cells grown on the CoL scaffold were used as a control. The measurements were performed in triplicate for each group ($n = 3$). Cell proliferation trends were drawn accodring to cell culture time and the OD value.

Cell osteogenic induction. The hBMSCs cells were cultured on 3D scaffolds with PM for 24 h. Osteogenic induction was conducted. For inducing osteogenesis, osteogenic-induction medium (OM) comprising 10 mM β-glycerophosphate, 100 nM dexamethasone, and $200 \, \mu M$ ascorbic acid was used. The OM was replaced every other day. After 7 days of culturing, alkaline phosphatase (ALP) staining was used to detect the differences of the expression in each group. The cells total RNA was also extracted to test the impact of osteogenesis gene expression differences of each printed scaffold to cells.
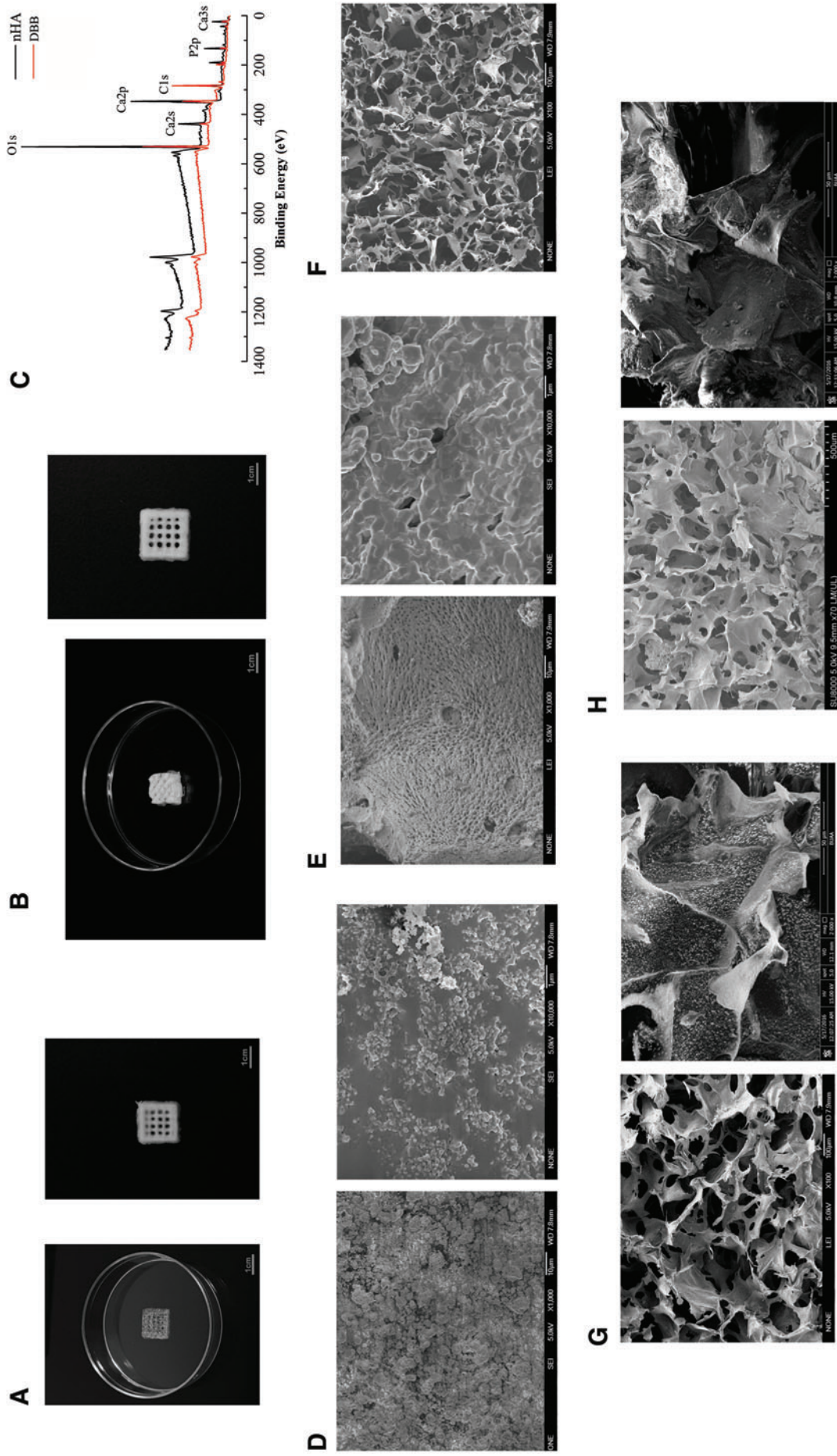
FIG. 1. **(A, B)** are the gross view of the surface morphology of the experimental nHA/CoL and DBB/CoL composite scaffolds, respectively; **(C)** XPS patterns of nHA and DBB, respectively; **(D, E)** the SEM images of nHA and DBB, respectively; (*Inset* to each image is the corresponding pattern); **(F, G, H)** are the SEM images of bioprinted tissue construct of CoL, nHA/CoL, and DBB/CoL, respectively (*Inset* to each image is the corresponding lyophilized pattern). DBB, deproteinized bovine bone; nHA, nano hydroxyapatite; CoL, collagen; SEM, scanning electron microscopy; XPS, X-ray photoelectron spectroscopy. Color images are available online.

TABLE 1. THE PRINTING PARAMETERS OF THE THREE-DIMENSIONAL BIOPLOTTER

Parameters	Temperature (°C)	Needle description (mm)	Pressure (bar)	Speed (mm/s)	Platform temperature (°C)
Reference value	4–10	0.25	2.0–3.0	10.0	4

ALP staining. The level of ALP activity was examined on day 7 using an ALP kit (Corning Incorporated) according to the manufacturer's protocol. The medium in each well was aspirated and, then, fixed with 95% ethanol for 30 min. Counterstaining consisted of BCIP, NBT, and buffer at a rate of 1:1:38 and was added to each well with a volume of 500 μL for 30 min in the dark. The staining solution was aspirated and washed with PBS three times. Record the results of ALP staining under the inverted phase contrast microscope.

Quantitative real-time polymerase chain reaction assay

Cells cultured on printed 3D constructs for 7 days were analyzed for gene expression ($n = 3$). Total RNA was extracted using TRIzol reagent (Invitrogen) by following the manufacturer's protocol. SYBR FAST qPCR Kit Master Mix (2BR; KAPA Biosystems) was used for quantitative Real-time PCR, and the HiFiScript Rapid De-Genomic cDNA First-Chain Synthesis Kit (Corning Incorporated) was used for reverse transcription. The target PCR primers for Runt-related transcription factor (*RUNX2*), Osteocalcin (*OCN*), SRY-related HMG box gene 9 (*SOX9*), and Collagen I a1 (*COLIA1*) were synthesized by Invitrogen (Table 1). β-Actin was used as an internal standard. The cycle threshold values (Ct values) were used to calculate the fold differences by the Ct method (also known as the $2^{-\triangle\triangle Ct}$ method).

Statistical analysis

Data are represented as the mean ± standard deviation and were analyzed using SPSS 17.0 software. In terms of statistical comparison, this study adopted the *t*-test and after confirmation of homogeneity of variance, one-way ANOVA as well as the LSD test were performed. The significance level was $\alpha = 0.05$. $*p < 0.05$ was considered to indicate statistical significance.

Results

Physical and chemical properties of printed 3D scaffolds

XPS analysis. The XPS spectrum in Figure 1C exhibits the characteristic elements of Ca, P, O, and C elements in nHA and DBB crystal. The diffraction peaks were analyzed using CASA XPS software and the Ca/P ratio calculated. The result displayed that Ca/P ratio is 1.67 for nHA and 1.58 for DBB, both of which were consistent with those reported previously.[22–26] The Ca/P ratio in DBB is lower than in nHA possibly because the $Ca_{10}(PO_4)_6(OH)_2$ in the calf bone was partially converted to β-$Ca_3(PO_4)_2$ during the calcination process, resulting the Ca/P ratio in DBB less than 1.67 in hydroxyapatite.[9,10]

SEM of nHA and DBB. The surface morphology of the two HA under SEM is shown in Figure 1D and E. A few agglomeration particles were observed in nHA (Fig. 1D). While the surface images of DBB (Fig. 1E) exhibited the evenly distributed micropores, and few interconnecttions between the pores, which is similar with the nature bone trabecula. The micropore diameter from DBB was about 1 μm, which were not presented in nHA. Both nHA and DBB crystals were spherical and have similar diameters in the images inserted to (Fig. 1D, E).

The construction of 3D printed scaffold. The scaffolds printed were fabricated successfully as shown in Figure 1A and B. After printing, a grid-like structure was constructed. The diameter of up and down connected square hole is 600 μm. The DBB scaffolds were more feasible to bottom up a higher construction during the printing (Fig. 1B).

SEM of 3D printed scaffold. The surface morphology of the scaffold after being lyophilized under SEM is shown in Figure 1F–H. All the scaffolds had porous structure, and the pore size was ranged from 100 to 300 μm. The CoL scaffold (Fig. 1F) was presented an irregular lamellar structure and the heterogeneous pore distribution with pore size ranged from 60 to 300 μm, and a little deformation of the pores could be seen on collagen scaffold. The surface morphology of nHA/CoL and DBB/CoL scaffolds (Fig. 1G, H) showed the regular porous structure distributed. The images inserted to (Fig. 1G, H) were magnified to see the details of nHA/CoL and DBB/CoL scaffolds. nHA evenly distributed on the collagen surface due to the small particle, while the DBB particle could be clearly seen in DBB/CoL scaffolds surface.

FTIR analysis. Figure 2A and B show the FTIR spectra of the material and scaffolds. In nHA, the peaks at 3568.2 and 3440.5 cm^{-1} belong to the OH- stretching vibration of hydroxyl.[27] Furthermore, the major bonds associated with PO43-(1037, 603, and 567 cm^{-1}) appeared in nHA and DBB.[28] The peak at 3330–3428.6 cm^{-1} belongs to the $N = H$ stretching of Amide A. The peak at 1655 cm^{-1} is C=O absorption of Amide I, 1550 cm^{-1} is C-N stretching and C-H bending combination vibration of Amide II, while 1237 cm^{-1} is consist of C-N stretching, N-H bending and C-C stretching of Amide III.[29–31] From the FTIR spectra, the two composite scaffolds are consistent with vibration of PO_4^{3-} in 1037, 603, and 567 cm^{-1}. However, the peaks at 970 and 1127 cm^{-1} in DBB/CoL are the PO_4^{3-} absorption of TCP,[28] which were not presented in nHA/CoL scaffolds.

XRD analysis. The XRD analysis of the material and scaffolds is shown in Figure 2C and D. The crystalline phases of both nHA and DBB were consistent with the phases incorporated in the International Centre for Diffraction Data (ICDD) databases. The analysis of nHA and DBB was based on the $Ca_{10}(PO_4)_6(OH)_2$ phase (JCPDS No.41-0487).[31,32] Peaks at 8° and 21.08°in both scaffolds
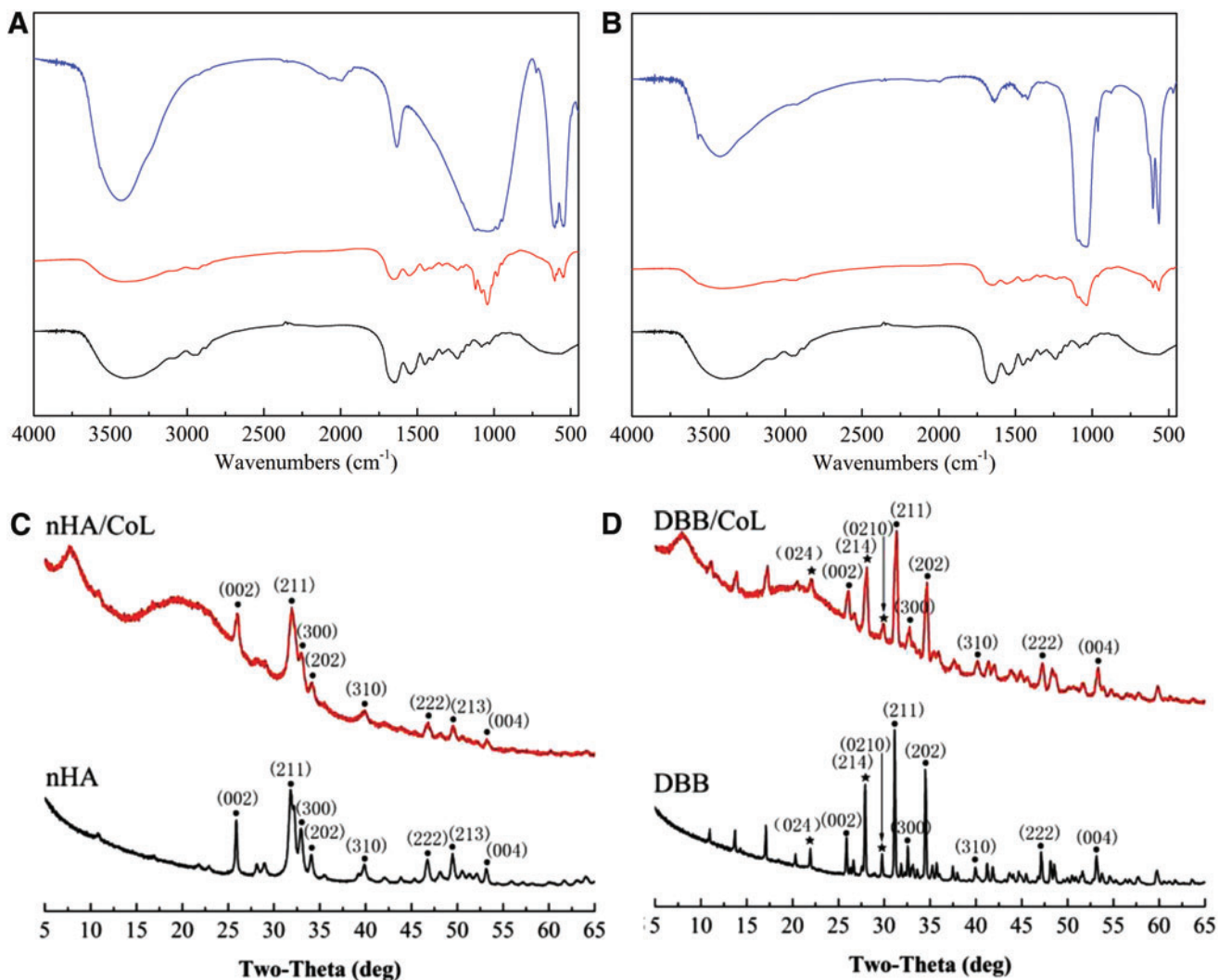
FIG. 2. **(A, B)** are the FTIR patterns of nHA, nHA/CoL, DBB, and DBB/CoL; *Dashed lines* indicate similar symbolic peaks of the two groups: $1037 \, cm^{-1}$: v3 vibration of $PO4^{3-}$; 606 and $562 \, cm^{-1}$: v4 vibration of $PO4^{3-}$; $1655 \, cm^{-1}$: Amide I; $1550 \, cm^{-1}$: Amide II; $1237 \, cm^{-1}$: Amide III. **(C, D)** are X-ray diffraction patterns of nHA, nHA/CoL, DBB, and DBB/CoL; The *black dots* in **(C, D)** represent the $Ca_{10}(PO_4)_6(OH)_2$ phases; The *black pentagram* in **(D)** represents the β-TCP phases. FTIR, Fourier transform infrared spectroscopy. Color images are available online.

were the diffraction reflecting the amorphous structure of collagen.[33] The main miller indices for TCP were (024), (214), and (0210), which were included in DBB as well as the DBB/CoL scaffold as shown in Figure 2D.[32]

Mechanical properties (Young's Modulus)

Young's Modulus of 3D printed scaffolds was detected as shown in Figure 3. The result clearly indicates that the Young's Modulus was 7.9 ± 0.3 MPa in nHA/CoL group that has significant differences when compared with 3.5 ± 0.4 MPa in CoL group ($p < 0.01$) and 4.5 ± 0.7 MPa in DBB/CoL group ($p < 0.05$), respectively. The difference between CoL and DBB/CoL group was not obvious.

CLSM analysis of hBMSCs on 3D scaffolds. FITC-phalloidin, vinculin, and DAPI staining (Fig. 4A–C) revealed that hBMSCs were firmly adhered to the scaffolds after 24 h seeding. The FITC-phalloidin and DAPI staining indicated that cells distributed on the skeleton structure and inner sides of the

scaffolds. The specific triple helix of the collagen as well as the porous structure of the scaffolds made a strong adsorption of phalloidin leading the scaffolds dyed as green, while the cell microfilaments were not stained, and the pore-size and porosity of scaffolds can be reflected due to the fluorescent staining.

Vinculin staining (Fig. 4D–F) showed that hBMSCs cells attached scaffolds well. The cellular pseudopods can be clearly seen in images. Cell adhesive plaques were evenly distributed in the cytoplasm and enriched at the end of cell pseudopodia, which showed enhanced fluorescence signal. The cells on the nHA/CoL and DBB/CoL scaffolds altered to a plate-like morphology in contrast to the spindle morphology observed on CoL scaffolds. The white boxes (Fig. 4E, F) represented nHA and the degradation particles of DBB, respectively. The cells can be seen well grown around the HA parties in scaffolds.

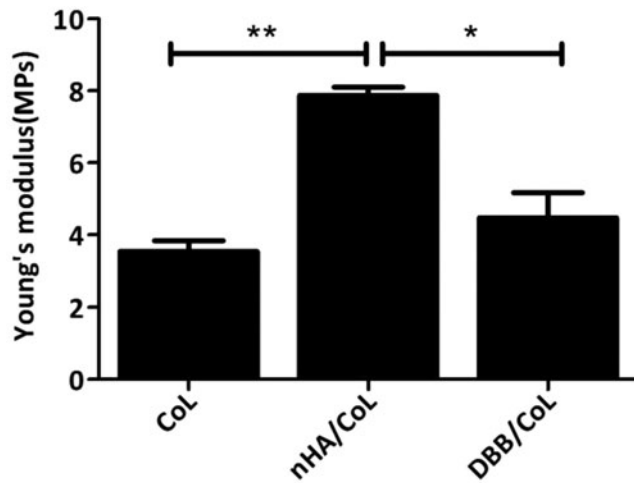Proliferation of hBMSCs in 3D scaffolds. The cells proliferation in different scaffolds was evaluated by CCK-8 assay

FIG. 3. Young's moduli of CoL, nHA/CoL, and DBB/CoL group (*$p < 0.05$; **$p < 0.01$). The Young's moduli of nHA/CoL was significantly stranger then CoL (**$p < 0.01$) and DBB/CoL scaffold (*$p < 0.05$), respectively; DBB/CoL was stranger then CoL scaffold (*$p < 0.05$).

at 1, 3, 5, and 7 days after seeding as shown in Figure 5. The OD values of all groups increased over time. The growth curves indicated that the overall growth tendencies in both groups were similar during the culture process. However, the cell proliferation was higher in CoL group than in nHA/CoL and DBB/CoL group at 5th and 7th day ($p < 0.05$). The cells proliferation on nHA/CoL and DBB/CoL was consistent and had no significant difference ($p > 0.05$).

ALP staining. The osteogenic potential of hBMSCs in different scaffolds was evaluated by ALP staining as shown in Figure 6. After 7 days of culturing, the result showed that cells in PM did not display significantly staining (Fig. 6A–C), while cells in OM showed positive ALP staining

(Fig. 6D–F). The brown spindle morphology in red dashed box (Fig. 6D–F) represented the expression of ALP in MSCs cells, respectively. Cells in PM showed more obvious proliferation effect, and the numbers of hBMSCs cells in PM were greater than that in OM group.

Osteogenesis-related gene expression in hBMSCs. Osteogenesis-related gene expression could reflect the differentiation of hBMSCs into osteoblasts. After the culture of hBMSCs on three groups of scaffolds for 7 days, the mRNA levels of osteogenesis-related genes of *OCN, RUNX2, SOX9,* and *COLIA1* were detected using real-time polymerase chain reaction (RT-PCR), and the results are shown in Figure 7. As the results display, the osteogenesis-related genes expression in OM group are significantly higher than the parallel group dealt with PM ($p < 0.01$). In OM group, the expression of *SOX9, OCN,* and *COLIA1* gene in hBMSCs cultured in nHA/CoL scaffolds is significantly higher than that in CoL scaffolds ($p < 0.05$). The *RUNX2* expression in nHA/CoL scaffolds is lower than that in CoL and DBB/CoL scaffolds ($p < 0.05$). The expression of *OCN* and *COLIA1* in DBB/CoL scaffolds was higher than that in CoL ($p < 0.05$). Transcription level had no significant difference between the gene of *RUNX2* and *SOX9* in the OM group in CoL and DBB/CoL scaffolds ($p > 0.05$). In PM group, there was no obvious difference in *OCN* expression among the three groups of scaffolds. The expression of *RUNX2* and *SOX9* was higher in PM group in DBB/CoL scaffolds than the same set of that in CoL and nHA/CoL scaffolds, respectively. At day 7, the expression level of *COLIA1* in CoL scaffolds was higher than that in nHA/CoL and DBB/CoL scaffolds in PM group ($p < 0.05$).

Discussion

Hydroxyapatite is a primary focus for synthetic bone graft substitutes because they are osteoconductive and provide sufficient mechanical strength.[25] Both nHA and DBB offer several biological advantages as a bone analog, and the HA-
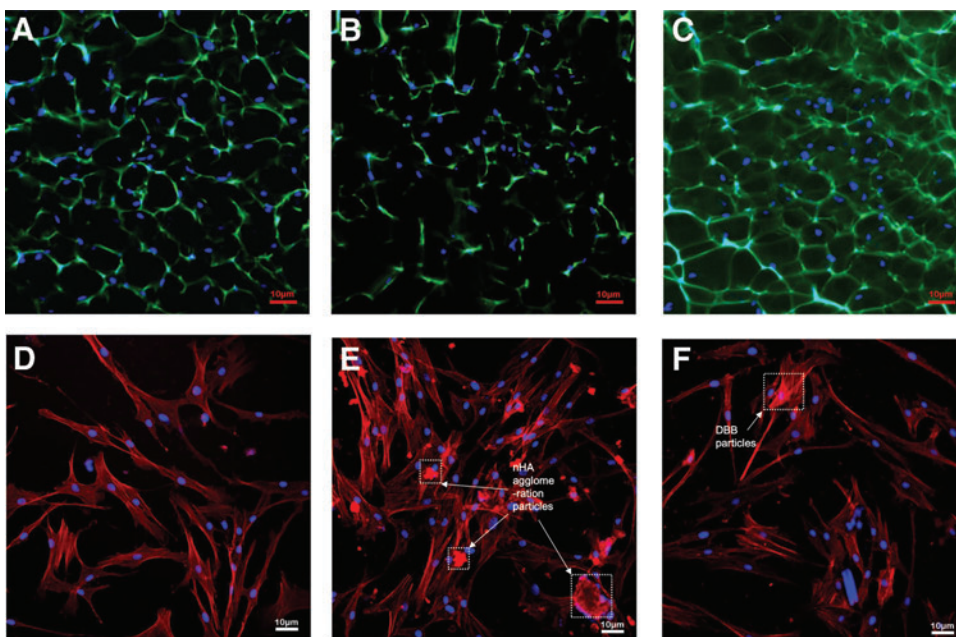

FIG. 4. Immunofluorescent staining for DAPI-stained nuclei of cells in 3D constructs after day 1; **(A–C)** represent CoL, nHA/CoL, and DBB/CoL 3D constructs, respectively, indicating the cellular 3D spatial distribution on day 1(40×); **(D–F)** are immunofluorescent staining for vinculin of cells in CoL, nHA/CoL, and DBB/CoL 3D constructs on day 1 after printing (40×), respectively. The *white boxes* in **(E)** and **(F)** represented nHA and the degradation particles of DBB, respectively. Scale bar: 10μm. Color images are available online.
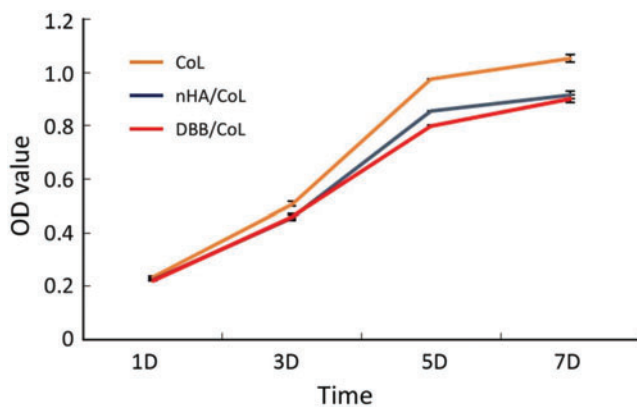
FIG. 5. hBMSCs proliferation on scaffolds using the CCK8 assay at 1, 3, 5, and 7 days after seeding. hBMSC, human bone marrow-derived mesenchymal stem cell. Color images are available online.

collagen composition has been widely applied in clinics as a commercial product.[7,9,33–35] Although a variety of materials have been processed into porous 3D scaffolds using various 3D technologies,[36–39] the nHA and DBB materials have not previously been mixed with collagen into hydrogel and printed into 3D scaffolds. In this study, two kinds of hydroxyapatite, nHA and DBB, were mixed with collagen, respectively, and printed into specific forms to compare the physical characteristics and the osteogenesis-promoting effects on hBMSCs and to determine a potential candidate for future studies in clinical application.

Three-dimensional bioprinting technology has the advantage of ''personal customization'' over molding or paste injection, including patient-specific geometries[7] and controlled spatial patterning of drugs or polymers within the scaffold.[8] To achieve this aim, the physical properties of the materials, such as powder granularity, roughness, wettability, or binder viscosity, must satisfy the demands of the complexity of 3D printing, which limits the types of materials that can be printed at low temperature.[40] In this article, a powder of nHA and DBB mixed with Type I collagen was printed into a 3D scaffold, while pure collagen scaffolds served as control group. Based on previous research, glutaraldehyde was ap-

plied for crosslinking to enhance the mechanical properties and maintain the structure of the scaffolds.[23]

The XPS analysis showed the element composition of the two inorganic materials. The elemental ratio of the two inorganic materials is consistent with what has been previously reported.[21,41] The FTIR and XRD analysis confirmed that there is a single ingredient—hydroxyapatite in nHA, while there is not only existence of the HA but also β-TCP in DBB. The DBB degrades and resolves faster compared to HA because of the high biodegradation rate and solubility of β-TCP.[23] With the β-TCP degradation, the calcium ions and phosphate released can promote osteogenesis by favoring the synthesis of osteoinductive growth factors and by upregulating adenosine signaling in phosphate[9,42,43] metabolism. Some literature has reported that HA and β-TCP composites have a better osteogenesis effect than using HA only.[8,41]

Excellent mechanical properties not only provide a mechanical support for bone formation but also make the materials conducive for use in clinical applications.[21] Young's moduli of bioinks were examined before being printed into tissue constructs with the bioprinter. The compressive modulus of the scaffolds is 7.9 ± 0.3 MPa in nHA/CoL group and 4.5 ± 0.7 in DBB/CoL group, both of which match that of cancellous bone (about 2–20MPa).[9,32,33] The compressive modulus of nHA/CoL and DBB/CoL scaffolds was higher than that in the group of CoL scaffolds, which illustrates that both nHA and DBB can enhance the compressive modulus of collagen. The phenomenon occurred because of collagen's affinity to Ca^{2+} as well as crosslinking of using glutaraldehyde, which can increase the mechanics of collagen by increasing its resistance to fibril rotation.[23,34] Collagen plays a role in crystallizing and mineralizing templates during the process of HA crystallization, and has the function of guiding the distribution of HA particles along the surface of collagen fibers.[44] Meanwhile, the combination of collagen and Ca^{2+} in the material have possibility to mineralize the collagen fiber and thus may increase the Young's modulus of the composite scaffolds.[45] nHA has a smaller particle size than DBB, and therefore has a larger surface area, making the Ca^{2+} easy to dissolve into collagen. Hence, nHA/CoL has higher compressive modulus than the other two groups.

After the composite ''bioink'' was printed into 3D scaffold by the 3D bioprinter, a specific architecture was built

FIG. 6. ALP staining of hBMSCs on scaffolds 7 days after seeding (100×). **(A–C)** represent cells on CoL, nHA/CoL and DBB/CoL scaffolds in proliferation medium (PM) did not display significant ALP staining, **(D–F)** represent cells on CoL, nHA/CoL and DBB/CoL scaffolds in osteogenic-induction medium (OM) showed positive ALP staining. The brown spindle morphology in *red dashed box* **(D–F)** represented the expression of ALP in MSCs cells, respectively.
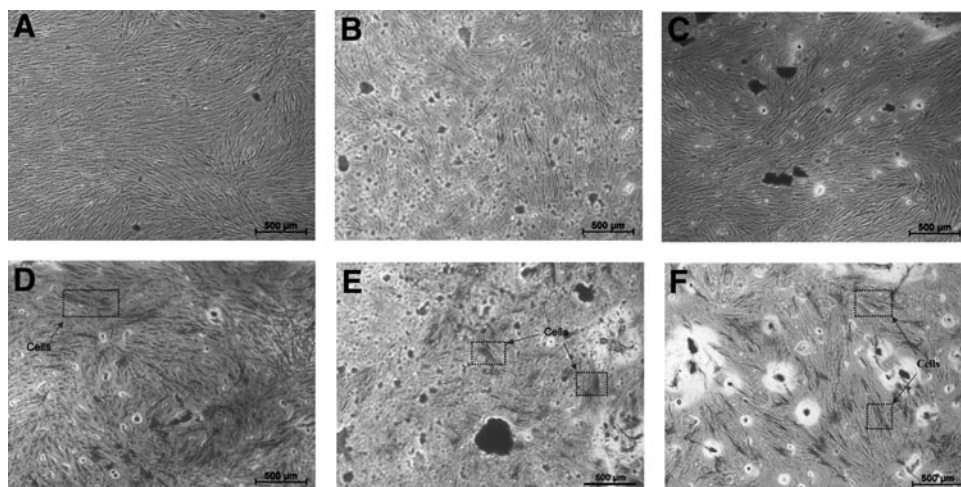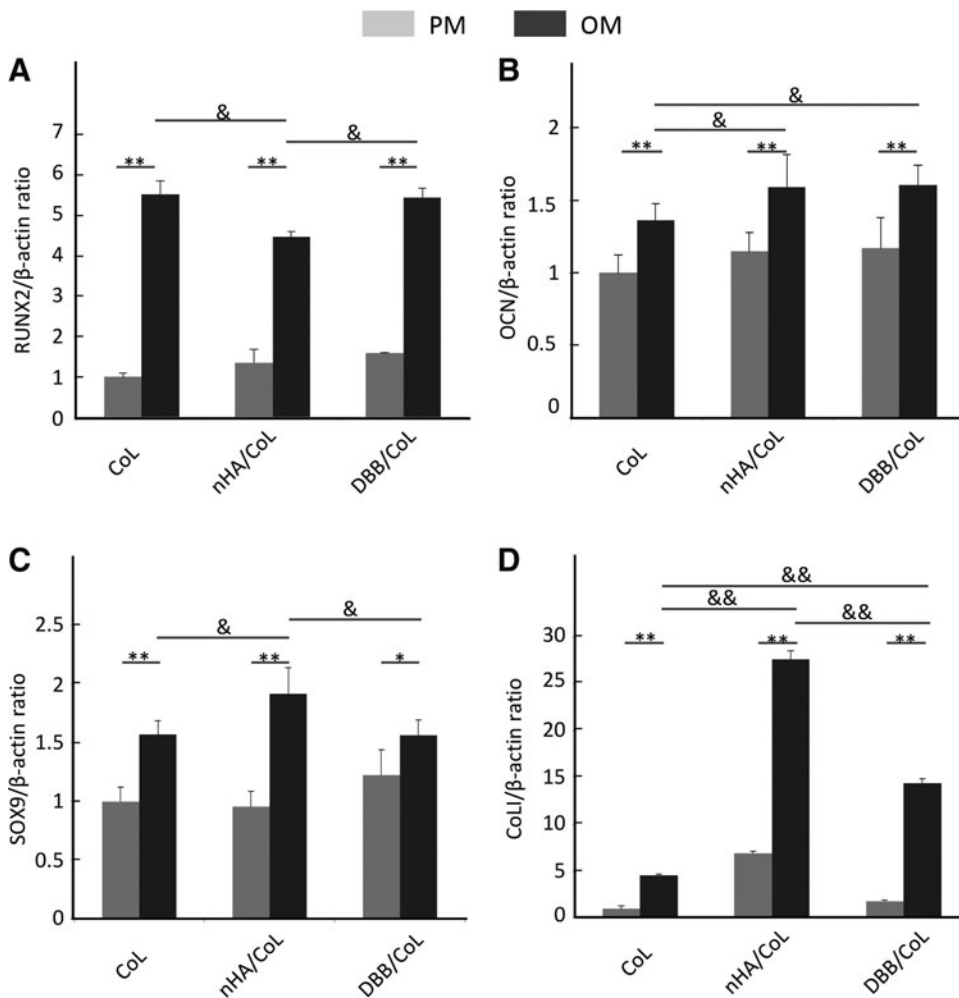
FIG. 7. Expression of *RUNX2* (**A**)*, OCN* (**B**)*, SOX9* (**C**)*,* and *COL* (**D**) genes in hBMSCs cultured in PM or OM. ("*" represent *t*-test between PM and OM group,*$p < 0.05$, **$p < 0.01$; "&" represent *t*-test between two PM groups, &$p < 0.05$, &&$p < 0.01$). OM, osteogenic-induced medium; PM, proliferation medium.

up. After being printed, the 3D scaffold had a grid-like microstructure with pore widths of 600 μm. Due to this porous structure, the DBB scaffolds were more feasible to bottom up a higher construction during the printing. The SEM analysis after lyophilization showed that both of the bioprinted scaffolds have a relatively smooth surface, due to the compression of the tip mold and nozzle. Internally, the scaffold presented the typical characteristics of cancellous bone, a honeycomb microstructure evenly distributed with 100 μm pores. The pores are assumed to be created by the sublimation of the solvent during lyophilization.[46] The high-resolution SEM images of nHA/CoL reflected the uniform particle distribution of nHA, which resulted in a more integrated structure. As to the DBB particles, because of the particle size and the internal pores, BDD/CoL group presented a porosity structure, including the micropores inside the materials and the macropores fabricated by the 3D printers.

A series of studies have demonstrated that the mineral properties, including solubility, chemical composition, and surface morphology were important factors for regulating diverse cell behaviors.[36–38] The different properties of the two inorganic parameters may have a diverse effect on cell behavior. The hBMSCs have obvious multipotent differentiation abilities and are the most common cells in bone tissue engineering.[7,22,23] In this study, hBMSCs were used to detect the effect of the two inorganic materials on the osteogenic differentiation.

The FITC-phalloidin/PI staining intuitively displayed the growth and distribution of cells on 3D bioprinted constructs. The number of cells in the collagen scaffold group was higher than that of the other two groups. The two sets of printed scaffolds have larger pore size than the collagen group, which caused a lower seeding efficiency, consistent with other research.[41] Assessment of the biosafety of scaffolds is of primary importance. Vinculin staining and CCK-8 assay demonstrated that the bioprinted scaffolds were nontoxic to hBMSCs *in vitro*. Vinculin staining results proved that vinculin was expressed around almost all cells, which indicated that hBMSCs could show adhesive growth in both the collagen matrix and the composite matrix and illustrated that the adhesion ability was similar on all three types of scaffolds. The CCK-8 assay results indicated that the cells still had proliferative capacity in the bioprinted matrix material. After 3 days of incubation, the cells in collagen group had a significant proliferative effect compared with the composite group. The difference might be caused by the lower seeding efficiency in the nHA/CoL and DBB/CoL group as mentioned above. Moreover, the ions from disintegrated inorganic materials, such as Ca^{2+} and PO_4^{3-} and so on, might influence the OD values. ALP staining is an indicator reflecting the ability of osteoblastic differentiation of hBMSCs. After 7 days in OM, hBMSCs showed positive ALP staining, while the PM group did not show significant positive tests results, consistent with the previous report.[23]

The genes related to osteogenic differentiation, including *RUNX2, OCN, SOX8,* and *COLIA1,* have always been considered an important factor in early osteogenic differentiation, while *SOX9* and *OCN* are marker proteins in late osteogenic differentiation.[41,42] CoLI are important components of the ECM. The expression of *COLIA1* increased, indicating an increase in the synthesis of nonmineralized ECM, which is an important step in bone formation.[9,11] The RT-PCR results indicate that the expression of the osteogenic differentiation-related genes *RUNX2, OCN, SOX8,* and *COLIA1* in the OM groups were significantly higher than that in all the PM groups. The *RANKL/OPG* balance regulated by osteoclast/osteoblast interactions plays a key role in bone regeneration. The relative expression ratio of *RUNX2* in the nHA/Col group was lower than the ratio of CoL and DBB/CoL in the OM group. The *OCN* and *COLIA1* expression in DBB/CoL was significantly higher than in the CoL group. The results in the PM group were consistent with the OM. The osteogenic differentiation-related genes *SOX9* and *COLIA1* in hBMSCs have higher expression in the nHA/CoL and DBB/CoL groups than in CoL group after 7 days of incubation, especially in the nHA/CoL group, which indicated that Ca^{2+} released by nHA promoted osteoblast proliferation and the expression of osteogenic genes.[9]

From the above, the DBB were originally from natural bone, and the micro- and macroporous structures were a benefit to vascularization during bone defect repair. To obtain the best applicable ratio, and explore the most biomimetic natural bone for clinical application of the printing process, the difficulties of the particle size and irregular shape of this trabecular bone graft were overcome in this study.

Conclusion

Both two composite bioinks, nHA/CoL and DBB/CoL, were used to print biomimic 3D scaffolds successfully. The two kinds of hydroxyapatite composite which favor hBMSCs proliferation and differentiation proved to be promising candidates for a 3D scaffold bioink. A porous architecture was manufactured eventually. Further studies would need to be concentrated on the DBB as a bioink to build up a 3D printing customized bone substitute in clinical application.

Authors' Contributions

Qing Li and Xiongxin Lei equally contributed to this article. Peijun Lyu and Guifeng Zhang are corresponding authors.

Acknowledgment

Disclosure Statement

No competing financial interests exist.

References

 1. Provaggi, E., Leong, J.J.H., and Kalaskar, D.M. Applications of 3D printing in the management of severe spinal conditions. Proc Inst Mech Eng H **6,** 231, 2017.
 2. Noshin, M., Baker, H.B., Taskoy, E., *et al.* 3D printed biofunctionalized scaffolds for microfracture repair of cartilage defects. Biomaterials **185,** 219, 2018.
 3. Bruyas, A., Lou, F., Stahl, A.M., *et al.* Systematic characterization of 3D-printed PCL/β-TCP scaffolds for biomedical devices and bone tissue engineering: influence of composition and porosity. J Mater Res **14,** 33, 2018.
 4. Boga, J.C., Miguel, S.P., de Melo-Diogo, D., *et al.* In vitro characterization of 3D printed scaffolds aimed at bone tissue regeneration. Colloids Surfaces B Biointerfaces **165,** 207, 2018.
 5. Berzina-Cimdina, L., and Borodajenko, N. Research of calcium phosphates using Fourier transform infrared spectroscopy. In: Theophanides T, ed. Materials Science, Engineering and Technology, 2015, pp. 123–148.
 6. Camacho, N.P., West, P., Torzilli, P.A., *et al.* FTIR microscopic imaging of collagen and proteoglycan in bovine cartilage. Biopolymers **1,** 62, 2001.
 7. Lin, K.F., He, S., Song, Y., *et al.* Low temperature additive manufacturing biomimic three-dimensional hydroxyapatite/collagen scaffolds for bone regeneration. ACS Appl Mater Interfaces **11,** 8, 2016.
 8. Inzana, J.A., Olvera, D., Fuller, S.M., *et al.* 3D printing of composite calcium phosphate and collagen scaffolds for bone regeneration. Biomaterials **13,** 35, 2014.
 9. Wahl, D.A., and Czernuszka, J.T. Collagen-hydroxyapatite composites for hard tissue repair. Eur Cell Mater **1,** 11, 2006.
10. Zhou, H., and Lee, J. Nanoscale hydroxyapatite particles for bone tissue engineering. Acta Biomater **7,** 7, 2011.
11. Li, Q., Wang, T., Zhang, G.F., *et al.* A comparative evaluation of the mechanical properties of two calcium phosphate/collagen composite materials and their osteogenic effects on adipose-derived stem cells. Stem Cells Int **395,** 2016, 2016.
12. Vázquez, C.G., Barba, C.P., and Munguía, N. Stoichiometric hydroxyapatite obtained by precipitation and sol gel processes. Rev Mex Fis **3,** 51, 2005.
13. Kobayashi, K., Anada, T., Handa, T., *et al.* Osteoconductive property of a mechanical mixture of octacalcium phosphate and amorphous calcium phosphate. ACS Appl Mater Interfaces **24,** 6, 2014.
14. Li, L., Zhao, M., Li, J., *et al.* Preparation and cell infiltration of lotus-type porous nano-hydroxyapatite/polyurethane scaffold for bone tissue regeneration. Mater Lett **149,** 2015.
15. Krishnan, V., Bhatia, A., and Varma, H. Development, characterization and comparison of two strontium doped nano hydroxyapatite molecules for enamel repair/regeneration. Dent Mater **5,** 32, 2016.
16. Kikuchi, M., Itoh, S., Ichinose, S., Shinomiya, K., and Tanaka, J. Self-organization mechanism in a bone-like hydroxyapatite/collagen nanocomposite synthesized in vitro and its biological reaction in vivo. Biomaterials **13,** 22, 2001.
17. Ludwig, S.C., Kowalski, J.M., and Boden, S.D. Osteoinductive bone graft substitutes. European spine journal official publication of the Eur Spine J, the European Spinal Deformity Society, and the European Section of the Cervical Spine Research Society **9,** 1:2000.
18. Bohner, M. Calcium orthophosphates in medicine: from ceramics to calcium phosphate cements. Injury **10,** 4, 2000.
19. Wang, T., Li, Q., Zhang, G.F., *et al.* Comparative evaluation of a biomimic collagen/hydroxyapatite/β-tricaleium phosphate scaffold in alveolar ridge preservation with Bio-Oss Collagen. Front Mater Sci **2,** 10, 2016.
20. Liu, C., Han, Z., and Czernuszka, J.T. Gradient collagen/nanohydroxyapatite composite scaffold: development and characterization. Acta Biomater **2,** 5, 2009.
21. Bose, S., Vahabzadeh, S., and Bandyopadhyay, A. Bone tissue engineering using 3D printing. Mater Today **12,** 16, 2013.

22. Wang, X., Song, Y., Liu, Y., *et al.* Osteogenic differentiation of three-dimensional bioprinted constructs consisting of human adipose-derived stem cells in vitro and in vivo. PLos One **6,** 11, 2016.

23. Wang, X.F., Lu, P.J., Song, Y., *et al.* Nano hydroxyapatite particles promote osteogenesis in a three-dimensional bioprinting construct consisting of alginate/gelatin/hASCs. RSC Adv **8,** 6, 2016.

24. Klammert, U., Gbureck, U., Vorndran, E., *et al.* 3D powder printed calcium phosphate implants for reconstruction of cranial and maxillofacial defects. Journal of craniomaxillofacial surgery **8,** 38, 2010.

25. Vorndran, E., Klammert, U., Ewald, A., *et al.* Simultaneous immobilization of bioactives during 3D powder printing of bioceramic drug-release matrices. Adv Funct Mater **10,** 20, 2010.

26. Butscher, A., Bohner, M., Hofmann, S., *et al.* Structural and material approaches to bone tissue engineering in powder-based three-dimensional printing. Acta Biomater **3,** 7, 2011.

27. Chandran, P.L., Paik, D.C., and Holmes, J.W. Structural mechanism for alteration of collagen gel mechanics by glutaraldehyde crosslinking. Connect Tissue Res **4,** 53, 2012.

28. Perrien, D.S., Young, C.S., Alvarezurena, P.P., *et al.* Percutaneous injection of augment injectable bone graft (rhPDGF-BB and β-tricalcium phosphate [β-TCP]/bovine type I collagen matrix) increases vertebral bone mineral density in geriatric female baboons. Spine J **5,** 13, 2013.

29. Hoppe, A., Guldal, N.S., and Boccaccini, A.R. A review of the biological response to ionic dissolution products from bioactive glasses and glass-ceramics. Biomaterials **11,** 32, 2011.

30. Payne, K.J., and Veis, A. Fourier transform ir spectroscopy of collagen and gelatin solutions: deconvolution of the amide I band for conformational studies. Biopolymers **11,** 27, 1988.

31. Barth, A. Infrared spectroscopy of proteins. Biochim Biophys Acta **9,** 1767, 2007.

32. Autefage, H., Briandmésange, F., Cazalbou, S., *et al.* Adsorption and release of BMP-2 on nanocrystalline apatite-coated and uncoated hydroxyapatite/beta-tricalcium phosphate porous ceramics. J Biomed Mater Res Part B Appl Biomater **2,** 91, 2009.

33. Shih, Y.R., Hwang, Y., Phadke, A., *et al.* Calcium phosphate-bearing matrices induce osteogenic differentiation of stem cells through adenosine signaling. Proc Natl Acad Sci U S A **3,** 11, 2014.

34. Stachel, I., Schwarzenbolz, U., Henle, T., *et al.* Cross-Linking of Type I Collagen with Microbial Transglutaminase: identification of Cross-Linking Sites. Biomacromolecules **3,** 11, 2010.

35. Tenhuisen, K.S., Martin, R.I., Klimkiewicz, M., *et al.* Formation and properties of a synthetic bone composite: hydroxyapatite-collagen. Journal of biomedical materials research **7,** 29, 1995.

36. He, C., Xiao, G., Jin, X., *et al.* Electrodeposition on nanofibrous polymer scaffolds: rapid mineralization, tunable calcium phosphate composition and topography. Adv Funct Mater **20,** 20, 2010.

37. Specchia, N., Pagnotta, A., Cappella, M., *et al.* Effect of hydroxyapatite porosity on growth and differentiation of human osteoblast-like cells. J Mater Sci **3,** 37, 2002.

38. Chou, Y.F., Huang, W.B., Dunn, J., *et al.* The effect of biomimetic apatite structure on osteoblast viability, proliferation, and gene expression. Biomaterials **3,** 26, 2005.

39. Schwarz, M.L.R., Kowarsch, M., Rose, S., *et al.* Effect of surface roughness, porosity, and a resorbable calcium phosphate coating on osseointegration of titanium in a minipig model. J Biomed Mater Res Part A **3,** 89, 2009.

40. Koutsopoulos, S. Synthesis and characterization of hydroxyapatite crystals: a review study on the analytical methods. J Biomed Mater Res Part A **4,** 62, 2002.

41. Zhu, Y., Zhu, R., Ma, J., *et al.* In vitro cell proliferation evaluation of porous nano-zirconia scaffolds with different porosity for bone tissue engineering. Biomed Mater **5,** 10, 2015.

42. Ozeki, M., Kuroda, S., Kon, K., *et al.* Differentiation of bone marrow stromal cells into osteoblasts in a self-assembling peptide hydrogel: in vitro and in vivo studies. J Biomater Appl **7,** 25, 2011.

43. Legeros, R.Z. Properties of osteoconductive biomaterials: calcium phosphates. Clin Orthop Relat Res **395,** 395, 2002.

44. Ramirezrodríguez, G.B., Montesi, M., Panseri, S., *et al.* Biomineralized recombinant collagen-based scaffold mimicking native bone enhances mesenchymal stem cell interaction and differentiation. Tissue Eng Part A **23,** 23, 2017.

45. Zhang, W., Liao, S.S., and Cui, FZ. Hierarchical Self-Assembly of Nano-Fibrils in Mineralized Collagen. Chem Mater **16,** 15, 2003.

46. Poinern, G.E., Brundavanam, R.K., Mondinos, N., *et al.* Synthesis and characterisation of nanohydroxyapatite using an ultrasound assisted method. Ultrason Sonochem **4,** 16, 2009.

Address correspondence to:
Guifeng Zhang, PhD
State Key Laboratories of Biochemical Engineering
Institute of Process Engineering
Beijing 100190
China

E-mail: gfzhang@ipe.ac.cn